Accelerating Ions by Crossing Two Ultraintense Lasers in a Near-Critical Relativistically Transparent Plasma

Bin Liu,[1,2,3,*] Mingyuan Shi,[1,2] Matt Zepf,[1,2] Bifeng Lei,[1,2,4,†] and Daniel Seipt[1,2]
[1]Helmholtz Institute Jena, Fröbelstieg 3, 07743 Jena, Germany
[2]Institute of Optics and Quantum Electronics, Friedrich-Schiller-Universität Jena, 07743 Jena, Germany
[3]Guangdong Institute of Laser Plasma Accelerator Technology, Guangzhou, China
[4]Center for Applied Physics and Technology, HEDPS, and SKLNPT, School of Physics, Peking University, Beijing 100871, China

(Received 25 October 2021; revised 6 October 2022; accepted 15 November 2022; published 26 December 2022)

A new scheme of ion acceleration by crossing two ultraintense laser pulses in a near-critical relativistically transparent plasma is proposed. One laser, acting as a trigger, preaccelerates background ions in its radial direction via the laser-driven shock. Another crossed laser drives a comoving snowplow field which traps some of the preaccelerated ions and then efficiently accelerates them to high energies up to a few giga-electron-volts. The final output ion beam is collimated and quasimonoenergetic due to a momentum-selection mechanism. Particle-in-cell simulations and theoretical analysis show that the scheme is feasible and robust.

DOI: 10.1103/PhysRevLett.129.274801

A laser pulse propagating in plasma excites a comoving charge-separation field which enables effective trapped acceleration of charged particles [1]. Electrons in the laser-driven plasma wakefield have been accelerated to 7.8 GeV in 20 centimeters [2], showing promising prospects of laser electron acceleration. On the other hand, the positive part of the charge-separation field, which is usually referred as the snowplow field [3,4], is suitable for accelerating ions [3–9]. Currently, the laser intensity available in laboratories has already exceeded 10^{22} W/cm^2 [10–16]. Such a strong laser is capable of driving a snowplow field in near-critical relativistically transparent (NCRT) plasma with the strength greater than one teravolt per centimeter. Ions trapped in it can be accelerated to energies of multi-giga-electron-volts in tens of microns.

Similar to that in electron wakefield acceleration, how ions are trapped in the snowplow field is crucial to the acceleration process. Various schemes have been proposed in dealing with the trapping issue. Most of them put forward specific requirements on target configurations. Protons can be trapped when the plasma is mainly composed of heavy ions [3,4,17]. By adding a combined thin foil [18–21] or a microdroplet [22], ions in it can be preaccelerated and then trapped. Self-trapping of background ions happens at the boundary of the plasma when the plasma density is in a proper range [6,7,9]. However, as far as we know, it is still a challenge to produce a well-controlled well-designed near-critical density plasma target with the state-of-the-art target preparing technologies. New schemes with relaxed target requirements remain desirable.

With the advance of high-power lasers, two or multiple intense or ultraintense laser pulses are becoming available in more and more laboratories. This will bring new opportunities for various purposes, ranging from strong field photon-photon collision [23,24], to high-energy laser electron acceleration [25], and all-optical radiation sources [26–28]. Here, we show that the trapped acceleration of ions can be feasibly realized by simply crossing two ultraintense laser pulses in a NCRT plasma. An illustrative plot of the present scheme is shown in Fig. 1. One laser, we call it the trigger laser, is irradiated on the plasma from bottom and excites a shock, preaccelerating some of the background ions along the laser radial direction. Another laser, the driving laser, is irradiated from left and drives a comoving snowplow field which traps some of the preaccelerated ions. The fast moving snowplow field is stabilized by the background ions of the plasma and therefore can propagate for a relatively long distance, making it promising for accelerating ions to high energy. This may provide experimentalists an alternative to make trade-offs between the requirement of special designed targets and that of an additional setup of laser pulses.

We demonstrate the scheme with the help of two-dimensional (2D) particle-in-cell simulations by using EPOCH [29,30]. For simplicity, we use uniform hydrogen plasma and circularly polarized (CP) laser pulses with Gaussian envelopes in both space and time. The scheme also works for multi-ion-species plasma and linearly polarized (LP) lasers [31]. We first consider a case that both the driving laser and the trigger laser have the same parameters including peak laser intensity $I_d = I_t = 2.7 \times 10^{22}$ W/cm^2 (laser amplitude $a_d = a_t = 100$, the subscripts $_d$ and $_t$ are for the driving laser and trigger laser, respectively), wavelength $\lambda_L = 1$ μm, spot size $\sigma_d = \sigma_t = 4$ μm, and duration 33.3 fs. The plasma is uniformly distributed in the area $-20\ \mu\text{m} < x < 50\ \mu\text{m}$

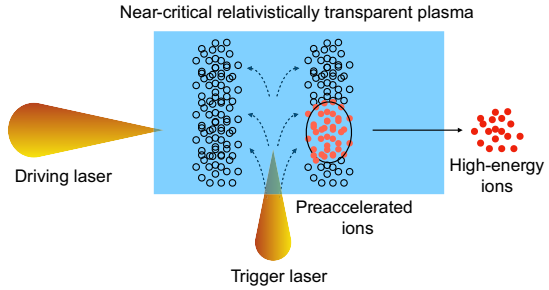

FIG. 1. Schematic plot. Two ultraintense laser pulses are crossed in a near-critical relativistically transparent plasma. One of them, the trigger laser (from bottom), preaccelerates background ions in its radial direction. Another one, the driving laser (from left), drives a snowplow field which traps and further accelerates some of the preaccelerated ions to high energy.

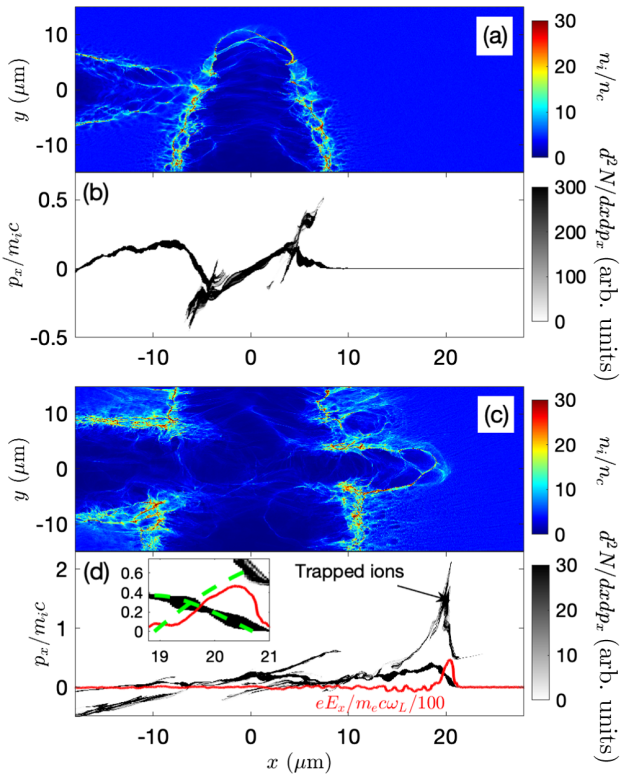

FIG. 2. Snapshots obtained from a 2D simulation by crossing two laser pulses in plasma. (a),(c) Ion density n_i/n_c and (b),(d) the phase space $(x - p_x)$ of ions along the axis of $y = 0$ (arbitrary unit) at different moments, (a),(b) 180 fs and (c),(d) 280 fs. The inset in (d) is a close-up of the accelerating bucket and the green dashed lines are predicted by Eqs. (2) and (3). The overlapping delay between the two laser pulses is 60 fs.

and $-17\ \mu\text{m} < y < 17\ \mu\text{m}$. We choose a relatively low plasma density $n_0 = 4n_c$ so that there is no self-trapping of background ions in the laser-driven snowplow field, where $n_c = m_e\omega_L^2\epsilon_0/e^2$ is the critical plasma density, $\omega_L = 2\pi c/\lambda_L$ the laser frequency, ϵ_0 the vacuum permittivity, m_e and e the mass and charge of electron, respectively, and c the speed of light in vacuum. The simulation box ranges from $-25\ \mu\text{m}$ to $75\ \mu\text{m}$ in the x direction and from $-20\ \mu\text{m}$ to $20\ \mu\text{m}$ in the y direction. The trigger laser is from the bottom along the axis of $x = 0$ and focused on $y = -17\ \mu\text{m}$ at 83 fs, while the driving one is from the left along $y = 0$ and focused on $x = -20\ \mu\text{m}$ at 133 fs. Both of the lasers drive plasma channels [Fig. 2(a)]. Ions initially off the channel axis experience shock acceleration in the radial direction which has attracted both theoretical and experimental interest since decades ago (e.g., [33–37]). At 180 fs, ions with momenta about $0.5m_ic$ along the x direction have been observed around the right side of the trigger laser [Fig. 2(b)], where m_i denotes the ion mass. Meanwhile, the front edge of the driving laser contacts the left side of the trigger laser. Later, at 280 fs, with the driving laser penetrating the channel of the trigger laser [Fig. 2(c)], some of the preaccelerated ions are caught by the snowplow field of the driving laser, experiencing a further trapped acceleration [Fig. 2(d)].

Eventually, a high density ion beam appears in the vacuum region at the rear side of the target, as is seen in Fig. 3(a). The most dense part, which is above $0.1n_c$ [Fig. 3(b)], is along the propagating axis $y = 0$. All the accelerated ions fly forward within a divergence angle about 25 degrees [0.45 rad, Fig. 3(c)] while the majority (also the most energetic ones) are within 10 degrees with a spectrum peak at about 2 GeV and an energy spread of about 500 MeV [Fig. 3(d)]. The peak energy and the beam quality are comparable to those in thin-foil radiation pressure acceleration regime which is believed to be promising in producing high-energy high-quality ion beams. For example, in Ref. [38], ion beams with peak energy up to 1.35 GeV, relative energy spread down to 15% and maximum divergence angle of about 10 degrees are observed in simulations with a similar laser energy. However, the beam quality in the thin foil radiation pressure acceleration regime can be significantly affected by the profile of the laser intensity. This makes it challenging to achieve high-quality ion beams in practical experiments (see, e.g., Ref. [39]). The beam quality in our scheme is more robust to the laser profiles.

We focus on the acceleration near the axis of the driving laser ($y \sim 0$) and within the accelerating bucket ($E_x > 0$). During the acceleration process, the propagating velocity of the laser front edge v_f varies slow in comparing with the variation of the ion velocities. This allows us to use a quasistationary approximation and introduce a one-dimension Hamiltonian [3,40], $H(\xi, p_x) = \gamma_i m_i c^2 - v_f p_x - \int q_i E_x(\xi) d\xi$, where $\xi = x - v_f t - \xi_0$, ξ_0 is a constant, p_x denotes the momentum of ions in the x direction, and $\gamma_i \approx \sqrt{1 + (p_x/m_ic)^2}$ the Lorentz factor of ions. Since the charge of the trapped ions is insignificant in comparing with that of the background ions, the electric

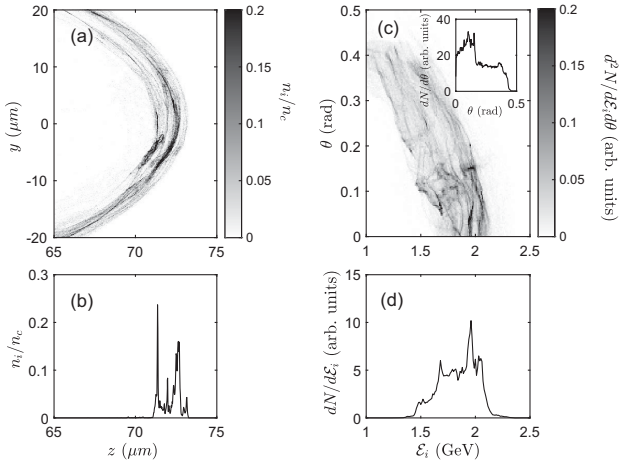

FIG. 3. The output ion beam at 467 fs obtained from the simulation in Fig. 2. (a) The density distribution (n_i/n_c) in space and (b) the line out at the axis $y = 0$. (c) The angular-energy distribution of ions, the angular distribution in the inset, and (d) the energy spectrum for ions within the divergence angle 10 degrees (arbitrary units).

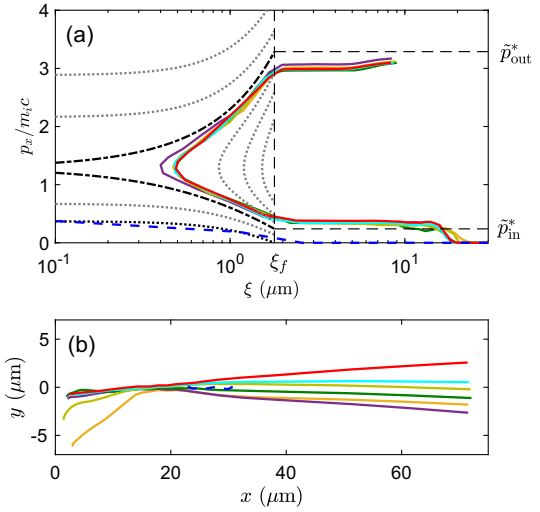

FIG. 4. The trajectories of six trapped ions (colored solid curves) and one untrapped ion (blue dashed curve) in (a) phase space ($\xi - p_x$) (see text) and (b) real space ($x - y$) tracked in the simulation in Fig. 2. The gray dotted curves in (a) depict the phase portrait of the Hamiltonian [Eq. (1)], the black dash-dotted and the black dotted curves are for the separatrix ($\mathcal{H} = -0.16$) and the background ions ($\mathcal{H} = 0$), respectively.

field E_x is mainly coupled with the background ions via quasistatic fluid equations [9,41], $(v_b - v_f)dp_b/d\xi = q_iE_x$, $dE_x/d\xi = q_in_b/\epsilon_0$, where $p_b = \gamma_b m_i v_b$, $\gamma_b = \sqrt{1 + (p_b/m_ic)^2}$, v_b, and $n_b = en_0/[q_i(1 - v_b/v_f)]$ denote the velocity and density of the background ions, respectively. Then the integral in the Hamiltonian can be expressed as $\int q_iE_x(\xi)d\xi = \gamma_b m_i(c^2 - v_fv_b) + C$, where C is an integral constant. By introducing $\mathcal{H} = (H - C)/m_ic^2$, $\beta = v/c$, and $\tilde{p} = p/m_ic$, we have

$$\mathcal{H}(\xi, \tilde{p}_x) = \sqrt{1 + \tilde{p}_x^2} - \beta_f\tilde{p}_x - [\gamma_b(\xi) - \beta_f\tilde{p}_b(\xi)]. \quad (1)$$

Under the nonrelativistic condition ($\gamma_b \sim 1$), $\tilde{p}_b(\xi)$ can be solved analytically [41],

$$\tilde{p}_b = \tilde{p}_{b,\max} - \frac{\beta_f}{2}\tilde{E}_x^2, \quad (2)$$

$$\tilde{E}_x = \chi^{1/3} - \frac{2(1 - \tilde{p}_{b,\max}/\beta_f)}{\chi^{1/3}}, \quad (3)$$

with $\chi = \eta + \sqrt{\eta^2 + [2(1 - \tilde{p}_{b,\max}/\beta_f)]^3}$, $\eta = 3\omega_i\xi/v_f$, $\tilde{E}_x = q_iE_x/m_iv_f\omega_i$, $\omega_i = \sqrt{q_ien_0/m_i\epsilon_0}$, and $\tilde{p}_{b,\max} = \tilde{p}_b(\xi = 0)$ is the maximum of $\tilde{p}_b$. The phase trajectory of the background ions corresponds to $\mathcal{H} = 0$ and touches the ground ($p_x = 0$) at $\xi = \xi_f$. The accelerating bucket is in the range $0 < \xi < \xi_f$ where $\xi_f = (v_f/\omega_i)[1 - 2\tilde{p}_{b,\max}/(3\beta_f)]\sqrt{2\tilde{p}_{b,\max}/\beta_f}$. The electric field peaks at $\xi = \xi_f$ as $\tilde{E}_{x,\max} = \sqrt{2\tilde{p}_{b,\max}/\beta_f}$. By comparing with the simulation shown in Fig. 2 in which the left boundary of the accelerating bucket is at about $x = 19$ μm at 280 fs, we have $\xi_0 = -47.5$ μm. By making use of the observed values $\beta_f = 0.79$ and $\tilde{p}_{b,\max} = 0.37$ the theoretical predictions of p_b and E_x are plotted in Fig. 2(d). They fit the simulation data roughly.

The Hamiltonian system contains a stable point ($\xi = \xi_f$, $\tilde{p}_x = \tilde{p}_f$) and an unstable point ($\xi = 0$, $\tilde{p}_x = \tilde{p}_f$), as is seen in Fig. 4(a), where $\tilde{p}_f = \gamma_f\beta_f$ and $\gamma_f = 1/\sqrt{1 - \beta_f^2}$. A trapping region around the stable point is delimited by a separatrix which corresponds to the Hamiltonian value $\mathcal{H}^* = 1/\gamma_f + \beta_f\tilde{p}_{b,\max} - \sqrt{1 + \tilde{p}_{b,\max}^2}$. The separatrix determines the minimum required incoming momentum $\tilde{p}^*_{\rm in} = \gamma_f^2[\beta_f(\mathcal{H}^* + 1) - \sqrt{\beta_f^2 + \mathcal{H}^*(\mathcal{H}^* + 2)}]$ and the corresponding maximum achievable output momentum $\tilde{p}^*_{\rm out} = \gamma_f^2[\beta_f(\mathcal{H}^* + 1) + \sqrt{\beta_f^2 + \mathcal{H}^*(\mathcal{H}^* + 2)}]$. When the snowplow field is strong enough so that $\tilde{p}_{b,\max} \to \tilde{p}_f$, one has $\mathcal{H}^* \to 0$ and $\tilde{p}^*_{\rm in} = 0$. This is the case that the separatrix coincides with the phase trajectory of the background ions. This corresponds to the threshold condition of self-trapping beyond which ions at rest can be trapped and accelerated [9]. As a contrast, in our simulation, the separatrix with $\mathcal{H}^* = -0.16$ is distinct from and higher than the trajectory of the background ions [Fig. 4(a)]. Only preaccelerated ions with incoming momenta larger than $\tilde{p}^*_{\rm in} = 0.24$ can be trapped. This results in a momentum selection mechanism which ensures a quasimonoenergetic and collimated output ion beam.

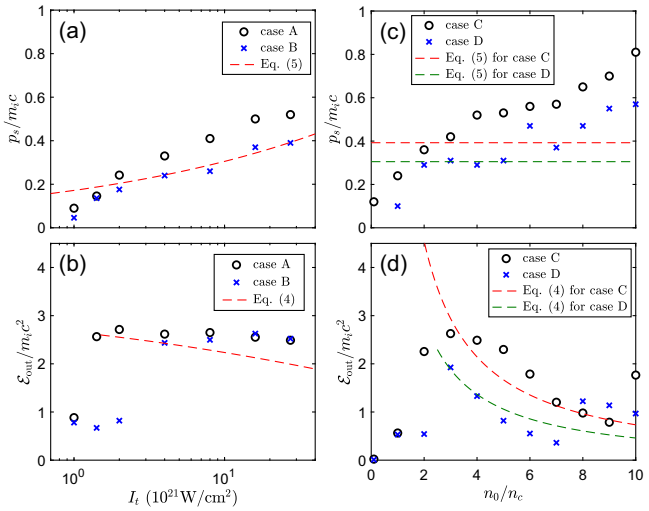

FIG. 5. (a) and (c) Maximum ion momentum along the axis of $y = 0$ in the preacceleration stage (p_s) and (b),(d) maximum final output ion energy ($\mathcal{E}_{out}$) versus (a),(b) peak intensity of trigger laser (I_t) for different trigger laser spot sizes, case A, $\sigma_t = 4$ μm (black circles) and case B, $\sigma_t = 2$ μm (blue crosses), and those versus (c),(d) plasma density n_0 for different laser intensities, case C, $I_d = I_t = 2.7 \times 10^{22}$ W/cm^2 (black circles) and case D, $I_d = I_t = 10^{22}$ W/cm^2 (blue crosses). Other parameters are the same as those used in Fig. 2. The dashed curves in (a),(c) and (b),(d) are theoretical predictions Eqs. (5) and (4), respectively.

Six trapped ions and one untrapped ion are tracked in the simulation. The trapped ions came from diverse initial positions [Fig. 4(b)] but are strongly calibrated later to a mainly forward track. The calibration appears to be caused by the radial charge-separation field generated by the driving laser. The ions are first preaccelerated from rest to momenta of $\sim 0.5 m_i c$ with the decrease of ξ until $\xi \sim 10$. The trapped acceleration happens when $\xi < 1.8$ and the final output momenta are $\sim 3 m_i c$. Although separated in space in the radial direction, the trapped ions merge in the phase space and flow along the phase trajectories of the Hamiltonian system roughly [Fig. 4(a)]. In contrast, the untrapped ion (initially at $x = 23$ μm, $y = 0$) flows along the phase trajectory of the background ions ($\mathcal{H} = 0$) and cannot be accelerated.

In simulations we have found that the peak energy of the ion beam remains similar even if the trigger laser is advanced or delayed by 20 fs. This is mainly due to the feature that the shock acceleration ends quickly so that the preaccelerated ions can wait for the snowplow field of the driving laser for a relatively long time period with almost unchanged velocities. This is practically important for experimental realization since an inaccuracy of the overlapping delay is usually inevitable, especially when two individual lasers are used. We have also found that the peak ion energy is almost the same by varying the focusing point of the driving laser from the boundary of the simulation box ($x = -25$ μm) to the crossing point ($x = 0$) along the axis of $y = 0$. Furthermore, the calibration of the direction of preaccelerated ions during the trapping process allows for a variation of the included angle between the two crossed lasers in a proper range. These features make the scheme proposed here practical and feasible.

In order to have a comprehensive understanding of the scheme, different laser plasma conditions have been considered in Fig. 5. Since the preacceleration stage driven by the trigger laser shock plays a crucial role, we plot not only the final output ion energy ($\mathcal{E}_{out}$) but also the preaccelerated momentum (p_s) as functions of laser plasma parameters. The former can be calculated from the Hamiltonian system as

$$\mathcal{E}_{out}/m_i c^2 = \gamma_f^2[\gamma_s(1 + \beta_f^2) - 2\tilde{p}_s\beta_f] - 1, \quad (4)$$

as long as $p_{in}^* < p_s < p_f$ is satisfied [42], where $\gamma_s = \sqrt{1 + \tilde{p}_s^2}$. The latter can be estimated as [34],

$$\tilde{p}_s \sim (2q_i m_e/e m_i)^{1/2}(I_t/1.37 \times 10^{18}\ \mathrm{W/cm^2})^{1/4}, \quad (5)$$

which meets the simulation data roughly, especially when the scheme works [Figs. 5(a) and 5(c)] [44]. The laser front edge velocity can be modeled as [45] $\beta_f = 1/\sqrt{1 + 2\pi^2 n_0/(f a_d n_c)}$, where f is introduced to account for the laser self-focusing effect. The theoretical prediction of $\mathcal{E}_{out}$ fits the simulation data of the maximum ion energy approximately by using $f = 1.35$ [Figs. 5(b) and 5(d)]. The scheme works even when I_t is as low as 1.4×10^{21} W/cm^2 [Figs. 5(a) and 5(b), case A], which corresponds to laser energy only a few percent of that of the driving pulse, indicating that the two-laser scheme can be implemented by modifying the one-laser self-trapping scheme without significantly increasing the energy cost of the entire laser system. The trigger laser energy can be further reduced by focusing the laser to a smaller spot size $\sigma_t = 2$ μm (case B) [46]. For the given lasers, the scheme works when the plasma density is high enough that $p_s > p_{in}^*$, but becomes inefficient when the density is so high that p_s is close to p_f. This determines an optimal range of plasma density which is $2 < n_0/n_c < 7$ for $I_d = I_t = 2.7 \times 10^{22}$ W/cm^2 [Fig. 5(d), case C] and $3 < n_0/n_c < 6$ for $I_d = I_t = 10^{22}$ W/cm^2 [case D]. Interestingly, self-trapping acceleration of background ions survives even with the presence of the trigger laser, resulting in efficient acceleration when the two-laser scheme is inefficient ($n_0/n_c = 10$ for case C and $n_0/n_c \geq 8$ for case D). Nevertheless, for a given driving laser, the maximum achievable ion energy via the two-laser scheme is higher than that via the self-trapping acceleration since v_f increases with the decrease of n_0. This is more pronounced when using LP lasers [31].

In summary, we have proposed a new scheme to generate high energy high quality ion beams by crossing

two ultraintense laser pulses in a NCRT plasma. It combines the shock acceleration of ions in laser radial direction and the trapped acceleration in laser-driven snowplow field. It extends the plasma density range used for laser ion acceleration in the NCRT regime. It requires bulk plasma targets with thickness larger than tens of microns and ultraintense laser pulses with duration longer than tens of femtoseconds, similar to that in the self-trapping acceleration regime in NCRT plasma. The two laser pulses can be produced either from two individual lasers directly or from one laser by inserting a beam splitter, e.g., a D-shaped mirror, into the beam line. The laser plasma interaction configuration can be implemented with feasible designs [31]. The ion dynamics observed in simulations is well described by an analytical model, indicating that the mechanism is simple and further investigation and optimization are possible. This Letter shows the potential of applying two or multiple ultra-intense laser pulses in ion acceleration which may be of great interest as such laser systems are becoming available.

We would like to acknowledge the Gauss Centre for Supercomputing (GCS) for funding this work by providing computing time through the John von Neumann Institute for Computing (NIC) on the GCS Supercomputer JUWELS at Jülich Supercomputing Centre (JSC). Bin Liu acknowledges Professor Wenjun Ma in Peking University for fruitful discussions and the support of Guangdong High Level Innovation Research Institute Project, Grant No. 2021B0909050006. Bifeng Lei acknowledges the support of the Science and Technology on Plasma Physics Laboratory, Grant No. 6142A04210110.

*liubin@glapa.cn
†b.lei@hi-jena.gsi.de

[1] T. Tajima and J. M. Dawson, Phys. Rev. Lett. **43**, 267 (1979).
[2] A. J. Gonsalves, K. Nakamura, J. Daniels, C. Benedetti, C. Pieronek, T. C. H. d. Raadt, S. Steinke, J. H. Bin, S. S. Bulanov, J. v. Tilborg *et al.*, Phys. Rev. Lett. **122**, 084801 (2019).
[3] O. Shorokhov and A. Pukhov, Laser Part. Beams **22**, 175 (2004).
[4] A. A. Sahai, F. S. Tsung, A. R. Tableman, W. B. Mori, and T. C. Katsouleas, Phys. Rev. E **88**, 043105 (2013).
[5] D. Habs, G. Pretzler, A. Pukhov, and J. Meyer-ter Vehn, Prog. Part. Nucl. Phys. **46**, 375 (2001).
[6] A. V. Brantov, E. A. Govras, V. F. Kovalev, and V. Y. Bychenkov, Phys. Rev. Lett. **116**, 085004 (2016).
[7] B. Liu, J. Meyer-ter Vehn, K.-U. Bamberg, W. J. Ma, J. Liu, X. T. He, X. Q. Yan, and H. Ruhl, Phys. Rev. Accel. Beams **19**, 073401 (2016).
[8] A. V. Brantov, P. A. Ksenofontov, and V. Y. Bychenkov, Phys. Plasmas **24**, 113102 (2017).
[9] B. Liu, J. Meyer-ter Vehn, and H. Ruhl, Phys. Plasmas **25**, 103117 (2018).
[10] V. Yanovsky, V. Chvykov, G. Kalinchenko, P. Rousseau, T. Planchon, T. Matsuoka, A. Maksimchuk, J. Nees, G. Cheriaux, G. Mourou *et al.*, Opt. Express **16**, 2109 (2008).
[11] A. S. Pirozhkov, Y. Fukuda, M. Nishiuchi, H. Kiriyama, A. Sagisaka, K. Ogura, M. Mori, M. Kishimoto, H. Sakaki, N. P. Dover *et al.*, Opt. Express **25**, 20486 (2017).
[12] Z. Guo, L. Yu, J. Wang, C. Wang, Y. Liu, Z. Gan, W. Li, Y. Leng, X. Liang, and R. Li, Opt. Express **26**, 26776 (2018).
[13] G. Tiwari, E. Gaul, M. Martinez, G. Dyer, J. Gordon, M. Spinks, T. Toncian, B. Bowers, X. Jiao, R. Kupfer *et al.*, Opt. Lett. **44**, 2764 (2019).
[14] J. W. Yoon, C. Jeon, J. Shin, S. K. Lee, H. W. Lee, I. W. Choi, K. H. T, J. H. Sung, and C. H. Ham, Opt. Express **27**, 20412 (2019).
[15] J. W. Yoon, Y. G. Kim, I. W. Choi, J. H. Sung, H. W. Lee, S. K. Lee, and C. H. Nam, Optica **8**, 630 (2021).
[16] P. Wang, Z. Gong, S. G. Lee, Y. Shou, Y. Geng, C. Jeon, I. J. Kim, H. W. Lee, J. W. Yoon, J. H. Sung *et al.*, Phys. Rev. X **11**, 021049 (2021).
[17] B. Shen, Y. Li, M. Y. Yu, and J. Cary, Phys. Rev. E **76**, 055402(R) (2007).
[18] L.-L. Yu, H. Xu, W.-M. Wang, Z.-M. Sheng, B.-F. Shen, W. Yu, and J. Zhang, New J. Phys. **12**, 045021 (2010).
[19] F. L. Zheng, S. Z. Wu, C. T. Zhou, H. Y. Wang, X. Q. Yan, and X. T. He, Europhys. Lett. **95**, 55005 (2011).
[20] F. L. Zheng, H. Y. Wang, X. Q. Yan, T. Tajima, M. Y. Yu, and X. T. He, Phys. Plasmas **19**, 023111 (2012).
[21] S. S. Bulanov, E. Esarey, C. B. Schroeder, S. V. Bulanov, T. Z. Esirkepov, M. Kando, F. Pegoraro, and W. P. Leemans, Phys. Rev. Lett. **114**, 105003 (2015).
[22] B. Shen, X. Zhang, Z. Sheng, M. Y. Yu, and J. Cary, Phys. Rev. ST Accel. Beams **12**, 121301 (2009).
[23] H. Gies, F. Karbstein, and C. Kohlfürst, Phys. Rev. D **97**, 036022 (2018).
[24] J. Q. Yu, H. Y. Lu, T. Takahashi, R. H. Hu, Z. Gong, W. J. Ma, Y. S. Huang, C. E. Chen, and X. Q. Yan, Phys. Rev. Lett. **122**, 014802 (2019).
[25] A. Debus, R. Pausch, A. Huebl, K. Steiniger, R. Widera, T. E. Cowan, U. Schramm, and M. Bussmann, Phys. Rev. X **9**, 031044 (2019).
[26] A. Giulietti, N. Bourgeois, T. Ceccotti, X. Davoine, S. Dobosz, P. D'Oliveira, M. Galimberti, J. Galy, A. Gamucci, D. Giulietti *et al.*, Phys. Rev. Lett. **101**, 105002 (2008).
[27] W. Yan, C. Fruhling, G. Golovin, D. Haden, J. Luo, P. Zhang, B. Zhao, J. Zhang, C. Liu, M. Chen *et al.*, Nat. Photonics **11**, 514 (2017).
[28] D. Seipt, V. Y. Kharin, and S. G. Rykovanov, Phys. Rev. Lett. **122**, 204802 (2019).
[29] T. D. Arber, K. Bennett, C. S. Brady, A. Lawrence-Douglas, M. G. Ramsay, N. J. Sircombe, P. Gillies, R. G. Evans, H. Schmitz, A. R. Bell *et al.*, Plasma Phys. Controlled Fusion **57**, 113001 (2015).
[30] W. J. Ma, I. J. Kim, J. Q. Yu, I. W. Choi, P. K. Singh, H. W. Lee, J. H. Sung, S. K. Lee, C. Lin, Q. Liao *et al.*, Phys. Rev. Lett. **122**, 014803 (2019).
[31] See Supplemental Material at http://link.aps.org/supplemental/10.1103/PhysRevLett.129.274801 for more details, which includes Ref. [32].

[32] L. Obst, S. Göde, M. Rehwald, F. E. Brack, J. Branco, S. Bock, M. Bussmann, T. E. Cowan, C. B. Curry, F. Fiuza *et al.*, Sci. Rep. **7**, 10248 (2017).
[33] W. B. Mori, C. Joshi, J. M. Dawson, D. W. Forslund, and J. M. Kindel, Phys. Rev. Lett. **60**, 1298 (1988).
[34] A. Pukhov, Z. M. Sheng, and J. Meyer-ter Vehn, Phys. Plasmas **6**, 2847 (1999).
[35] G. S. Sarkisov, V. Y. Bychenkov, V. N. Novikov, V. T. Tikhonchuk, A. Maksimchuk, S. Y. Chen, R. Wagner, G. Mourou, and D. Umstadter, Phys. Rev. E **59**, 7042 (1999).
[36] K. Krushelnick, E. L. Clark, Z. Najmudin, M. Salvati, M. I. K. Santala, M. Tatarakis, A. E. Dangor, V. Malka, D. Neely, R. Allott *et al.*, Phys. Rev. Lett. **83**, 737 (1999).
[37] M. S. Wei, S. P. D. Mangles, Z. Najmudin, B. Walton, A. Gopal, M. Tatarakis, A. E. Dangor, E. L. Clark, R. G. Evans, S. Fritzler *et al.*, Phys. Rev. Lett. **93**, 155003 (2004).
[38] B. Qiao, M. Zepf, M. Borghesi, and M. Geissler, Phys. Rev. Lett. **102**, 145002 (2009).
[39] I. J. Kim, K. H. Pae, I. W. Choi, C.-L. Lee, H. T. Kim, H. Singhal, J. H. Sung, S. K. Lee, H. W. Lee, P. V. Nickles *et al.*, Phys. Plasmas **23**, 070701 (2016).
[40] Z. Gong, Y. Shou, Y. Tang, R. Hu, J. Yu, W. Ma, C. Lin, and X. Yan, Phys. Rev. E **102**, 013207 (2020).
[41] B. Liu, J. Meyer-ter Vehn, H. Ruhl, and K.-U. Bamberg, Proc. SPIE **10240**, 1024005 (2017).
[42] Alternatively, the preacceleration stage can be described by another Hamiltonian based on the estimation in Ref. [34] and the trapping process can be regarded as the intersection of the two Hamiltonian separatrixes, see, e.g., [43].
[43] Z. Gong, Y. Shou, Y. Tang, and X. Yan, Phys. Rev. E **102**, 053212 (2020).
[44] Actually, in simulations p_s is also affected by other factors such as the trigger laser spot size and the plasma density. This can be interpreted as a result of the laser self-focusing effect.
[45] B. Liu, J. Meyer-ter Vehn, H. Ruhl, and M. Zepf, Plasma Phys. Controlled Fusion **62**, 085014 (2020).
[46] For the cases with $\sigma_t = 2$ μm, $I_t = 1.4 \times 10^{21}$ W/cm^2 and 2×10^{21} W/cm^2, the scheme does not work because the trigger laser pulses are exhausted prematurely. This can be overcome by using longer trigger laser pulses.